J Appl Electrochem (2013) 43:953–965
DOI 10.1007/s10800-013-0583-9

ORIGINAL PAPER

Outstanding electro-catalytic activity of Pt_x–$(RuO_y$–$CeO_2)_{1-x}$/C composites towards ethanol oxidation in acid media

Lorenna L. A. Souza · Gláucia R. O. Almeida · Lays S. R. Silva · Franciele O. F. Bergamaski · Álvaro S. Lima · Katlin I. B. Eguiluz · Giancarlo R. Salazar-Banda

Received: 13 March 2013 / Accepted: 27 June 2013 / Published online: 10 July 2013

Abstract Direct ethanol fuel cells are a key enabling technology for clean energy conversion; however, a major challenge is the determination of anode catalytic materials with high performance for complete ethanol oxidation. In this study, we synthesized binary $Pt_{0.50}$–$(CeO_2)_{0.50}$/C and $Pt_{0.50}$–$(RuO_y)_{0.50}$/C, as well as ternary Pt_x–$(RuO_y$–$CeO_2)_{1-x}$ catalysts ($x = 0.25$, 0.50, or 0.75) and ($y = 0$, +2, or +3) by the sol–gel method and compared them in the ethanol oxidation reaction. Transmission electron microscopy images revealed the small particle size of the prepared catalysts (2.1–2.5 nm). Cyclic voltammetry, chronoamperometry, derivative voltammetry, and potentiostatic polarization were employed to analyze the ethanol oxidation reaction on binary $Pt_{0.50}$–$(CeO_2)_{0.50}$/C and $Pt_{0.50}$–$(RuO_y)_{0.50}$/C and ternary Pt_x–$(RuO_y$–$CeO_2)_{1-x}$ catalysts, as well as Pt/C and Pt–Ru/C commercial catalysts, including some insights estimating a possible reaction mechanism. The results demonstrate, considering the activity outcomes approach, the highly superior performance of the $Pt_{0.25}$–$(RuO_y$–$CeO_2)_{0.75}$/C catalyst.

Keywords Electrocatalysts · Direct ethanol fuel cell · Nanoparticles · Sol–gel method · Derivative voltammetry

1 Introduction

The prediction of energy shortage and environmental impacts caused by the excessive use of fossil fuels are forcing scientists to seek solutions to obtain energy through cleaner and more efficient technologies than those available at the moment [1]. Fuel cells which have very low or even zero emission of harmful greenhouse gases (e.g. CO_2, NO_x, SO_x, etc.), have generated great interest amongst the scientific and engineering communities [2–4]. Today, fuel cells are widely considered to be efficient and non-polluting power sources offering much higher energy densities and energy efficiencies compared to other current/conventional systems. The main advantages of these devices are the versatility of their applications and their high energy efficiency compared to the usual energy sources [5]. However, some disadvantages are nonetheless evident, such as the high cost and the difficulty of generating high power.

Proton exchange membrane fuel cells (PEMFC) based on the oxidation of small organic molecules [6] have attracted increasing attention in the scientific area, mainly for portable use. However, the current densities obtained are low since the kinetics of alcohol oxidation are slower in comparison with those of H_2 and there are also problems related to the effective diffusion of fuel to the cathode ("crossover") [7]. Hence, a major research challenge is to understand, at the atomic level, the reaction mechanism of alcohol electrochemical oxidation to design more efficient catalysts and to improve the chemical process of interest.

Therefore, remarkable efforts are required to create new anodic catalysts for direct alcohol fuel cells (DAFCs) containing small amounts of platinum that are capable of oxidizing primary and secondary alcohols with rapid kinetics and tolerable deactivation [8]. Platinum that is highly dispersed on a substrate (usually carbon with a high surface area) is commonly used for the electro-oxidation of these small organic molecules [3]. However, platinum-based electrocatalysts have high cost and also present a

L. L. A. Souza · G. R. O. Almeida · L. S. R. Silva · F. O. F. Bergamaski · Á. S. Lima · K. I. B. Eguiluz · G. R. Salazar-Banda (✉)
Instituto de Tecnologia e Pesquisa/Programa de Pós-Graduação em Engenharia de Processos, Universidade Tiradentes, Aracaju, SE 49032-490, Brazil
e-mail: gianrsb@gmail.com

gradual decrease in electrocatalytic activity over time [9]. Catalytic efficiency is influenced by the strong adsorption enthalpy of CO at active sites, causing catalytic poisoning and inhibiting further reactions [10, 11]. Therefore, the direct application of ethanol in fuel cells requires electrode materials with high electrocatalytic activity for both fuel oxidation and oxygen reduction [12, 13].

Numerous reports have studied Pt-based binary metal electrocatalysts for the anodic oxidation of alcohols [6–13]. However, a platinum–ruthenium (Pt–Ru) [14, 15] combination still remains the best choice for both PEMFC and DAFC, particularly at low temperatures. The activity and use of Pt needs to be improved by using modified Pt/C or Pt–Ru/C catalysts with appropriate promoters to decrease the dependence upon the loadings of anode catalysts to an economical level, without sacrificing their performance.

Ceria (cerium oxide) has received considerable attention as an oxide promoter [16]. Oxides of cerium have good stability and show high catalytic activity for CO oxidation intermediates produced during the oxidation of alcohols [17, 18]. Ou et al. [19] and Matolín et al. [20] reported that the electrochemical oxidation of methanol on a Pt–CeO_2/C catalyst in acid media showed improved performance compared to conventional catalysts.

Bai et al. [21] studied CO-stripping voltammograms taken using Pt–CeO_2/C and Pt–$Ce_{0.6}Zr_{0.4}O_2$/C catalysts, as well as Pt/C and Pt–Ru/C commercial catalysts. The peak potential of CO_{ads} oxidation was about 60–90 mV lower at Pt–CeO_2/C and Pt–$Ce_{0.6}Zr_{0.4}O_2$/C than that seen for Pt/C. Presumably, the metal oxide may favour the activation of water and/or OH species, and these chemisorbed oxygen species on the metal oxide surface promote CO_{ads} oxidation to CO_2 at lower potentials. Moreover, De Souza et al. [22] prepared Pt–CeO_2/C electrocatalysts at different mass ratios (3:1, 2:1, 1:1, 1:2, 1:3) by the polymeric precursor method for ethanol oxidation reaction. The Pt–CeO_2/C catalysts (except for Pt–CeO_2/C 1:1) exhibited improved performance when compared with Pt/C, especially the Pt–CeO_2/C 1:3 catalyst that also showed better results than the Pt–Ru/C (E-Tek) catalyst.

Considering that the use of ethanol is attractive, since it can be a renewable fuel and is less toxic than methanol, here, we evaluated and compared the ethanol oxidation reaction activity of carbon-supported binary $Pt_{0.50}$–$(CeO_2)_{0.50}$/C and $Pt_{0.50}$–$(RuO_y)_{0.50}$/C and ternary Pt_x–$(RuO_y$–$CeO_2)_{1-x}$ catalysts ($x = 0.25$, 0.50, or 0.75) with those of commercial Pt/C and Pt–Ru/C catalysts by employing voltammetric methods. The superior performance of $Pt_{0.25}$–$(RuO_y$–$CeO_2)_{0.75}$/C was attributed to the beneficial effects of the CeO_2 component and the presence of amorphous ruthenium oxides through a synergistic mechanism.

2 Experimental procedures

The catalysts were prepared according to a method described in the literature [23–26]. In brief, Pt/C (E-Tek Inc., USA) powder containing 10 % platinum was used as a support for co-catalyst deposition. The metal co-catalysts were deposited by dissolving the precursor metal (ruthenium acetylacetonate and/or ceric ammonium nitrate, all from Sigma-Aldrich) in a solvent containing isopropanol (Synth, 99.5 %) and acetic acid (Vetec, 99.7 %) in a 3:2 (v/v) ratio. All chemicals were of analytical grade and used without further purification.

Afterwards, an appropriate amount of Pt/C was added to the resulting sol and the mixture was homogenized in an ultrasonic bath (Ultracleaner 1450 A) for 30 min. The solvent was then slowly evaporated and the resulting powder submitted to thermal treatment at 400 °C for 1 h in a nitrogen atmosphere using a heating rate of 5 °C/min. Different amounts of the co-catalysts in the composites were calculated with respect to the amount of platinum catalytic powder. The catalysts Pt–RuO_y/C and Pt–CeO_2/C (with an atomic ratio of 1:1) or the Pt_x–$(RuO_y$–$CeO_2)_{1-x}$/C ternary catalytic composites were synthesized with a fixed atomic ratio between the elements Ru and Ce (1:1), though with an atomic ratio of 1:1, 3:1, and 1:3 between the Pt element and the Ru + Ce mixture. For comparison, some experiments were also carried out using Pt/C and $Pt_{0.50}$–$Ru_{0.50}$/C from E-Tek.

The electrochemical measurements were carried out in a standard two-compartment Pyrex® glass electrochemical cell using an Autolab potentiostat/galvanostat, type PGSTA T320N, coupled to a compatible microcomputer. All these operations were performed under a nitrogen atmosphere to prevent oxidation of the surface by contact with atmospheric oxygen.

The working electrode was prepared for all test systems by dissolving the catalytic composites in 200 μL of a 0.05 % Nafion® solution (Sigma-Aldrich) and 1,000 μL of Milli-Q water (Millipore). The resulting mixture was placed in an ultrasonic bath until it became homogeneous and then a layer of 20 μL of the mixture was deposited on a boron-doped diamond (BDD) electrode (geometric area: 0.55 cm^2), aiming for complete coating of the surface, then dried in air at 60 °C for 10 min. For all results presented here, a Pt plate of 1 cm^2 (each face) was used as a counter electrode. Selected experiments were performed at room temperature in 0.5 mol L^{-1} H_2SO_4 (Sigma-Aldrich, 98 %) aqueous solution as the supporting electrolyte, while for the ethanol electrochemical oxidation, 0.5 mol L^{-1} ethanol (Sigma-Aldrich, 96 %) solutions were used. The potentials were determined using a hydrogen electrode in the same solution (HESS) that was connected by a Haber–Luggin capillary and are referred to this electrode in the paper.

The activity of the catalysts was evaluated by cyclic voltammetry (CV recorded in the 0.05–1.50 V potential range), quasi-steady-state polarization curves (carried out in potentiostatic mode with all data points obtained after 300 s of polarization at each potential) and chronoamperometry (applying 600 mV for 600 s).

X-ray diffraction (XRD) patterns of the catalysts were obtained using a universal Carl Zeiss-Jena URD-6 X-ray diffractometer, operating with Cu Kα radiation ($\lambda = 0.15406$ Å) generated at 50 kV and 100 mA. The following parameters were kept constant during the X-ray analysis: 2θ range = 10°–100° with a step scan of 2° min^{-1}. The size of the nanoparticles was also investigated by transmission electron microscopy (TEM) using a Philips CM200 microscope operating at 200 kV. The samples were prepared by ultrasonically dispersing the catalyst powders in ethanol. A drop of the suspension was applied onto a carbon-coated copper grid and dried in air.

The metal atomic ratio of the different catalysts was determined by inductively coupled plasma-optical emission spectrometry (ICP-OES) in a Perkin-Elmer device, model Optimal 3000. For this purpose, the metal was extracted from the catalysts by refluxing them in an aqua regia solution for 8 h. The procedure was carried out in quadruplicate.

3 Results and discussion

3.1 Catalyst characterization

Figure 1a shows the XRD patterns of Pt/C (E-Tek) and of the synthesized electro-catalysts $Pt_{0.50}$–$(RuO_y)_{0.50}$/C, $Pt_{0.50}$–$(CeO_2)_{0.50}$/C, and $Pt_{0.50}$–$(RuO_y$–$CeO_2)_{0.50}$/C. The diffraction peaks at $2\theta \approx 39.8°$ (111), 46.2° (200), 67.5° (220), and 81.3° (311) are related to face-centered cubic platinum, which is consistent with the standard powder diffraction data for Pt (JCPDS 04-0802). The diffraction peaks at the Bragg angles of 28.5°, 56.3°, and 79.2° correspond to the (111), (311), and (420) facets of cubic CeO_2 (JCPDS 43-1002).

The diffraction peaks of $Pt_{0.50}$–$(RuO_y)_{0.50}$/C and, to a lesser degree, for $Pt_{0.50}$–$(RuO_y$–$CeO_2)_{0.50}$/C (better observed in Fig. 1b), shifted in relation to the platinum pattern, suggesting the presence of Pt–Ru alloys with the contraction of the crystalline lattice of Pt and consequent dislocation of the Bragg angles to higher values [27]. The (220) diffraction peak positions, the average crystallite sizes and the lattice parameters of all the catalysts are given in Table 1. The lattice parameters of all electrocatalysts containing ruthenium are smaller than those of Pt/C (0.3923 nm), probably due to the formation of a PtRu solid solution. Note that the lattice parameter of the $Pt_{0.50}$–$(CeO_2)_{0.50}$/C catalyst (0.3922 nm) is very close to the Pt/C parameter, indicating that none metallic cerium formed an alloy with Pt, remaining as CeO_2.

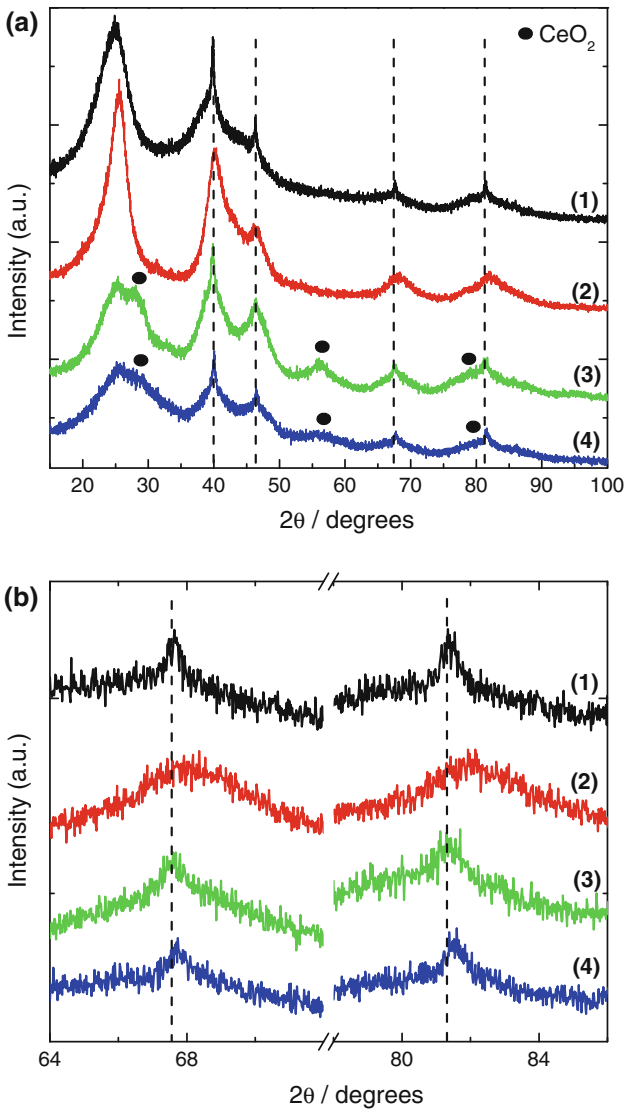

Fig. 1 **a** Continuous scan XRD patterns of the (*1*) Pt/C (E-Tek), and of the prepared electro-catalysts (*2*) $Pt_{0.50}$–$(RuO_y)_{0.50}$/C, (*3*) $Pt_{0.50}$–$(CeO_2)_{0.50}$/C, and (*4*) $Pt_{0.50}$–$(RuO_y$–$CeO_2)_{0.50}$/C. **b** an enlargement of a region from (**a**). *Vertical lines* in both figures correspond to pure polycrystalline Pt peak positions

However, in a previous report from our group, careful characterization of a catalyst containing Pt and Ru synthesized under the same conditions of this study (by the sol–gel method), demonstrated that Ru is also obtained in the amorphous RuO_2 form or still as RuO_3 to a lesser degree [18]. Thus, in the synthesized composites of this study, the ruthenium was designates as RuO_y ($y = 0$, +2, or +3).

Since the crystallite sizes of the ternary catalysts are almost the same (Table 1); then the different activities towards ethanol oxidation discussed hereafter are due to catalytic effect and not a particle size effect.

Table 1 Parameters taken from XRD measurements for the catalytic composites synthesized

Composite	(220) Diffraction peak position	Crystallite size from XRD/nm[a]	Lattice parameter/nm
Pt/C	67.53	2.4	0.3923
$Pt_{0.50}$–$(RuO_y)_{0.50}$/C	67.83	2.8	0.3908
$Pt_{0.50}$–$(CeO_2)_{0.50}$/C	67.55	3.1	0.3922
$Pt_{0.25}$–$(RuO_y$–$CeO_2)_{0.75}$/C	67.75	2.9	0.3801
$Pt_{0.50}$–$(RuO_y$–$CeO_2)_{0.50}$/C	67.63	2.9	0.3918
$Pt_{0.75}$–$(RuO_y$–$CeO_2)_{0.25}$/C	67.65	2.8	0.3917

[a] Mean crystallite size calculated using the WinFit 1.2 software

The TEM images shown in Fig. 2 demonstrate that the addition of Ru or Ce as co-catalysts to Pt does not significantly increase the particle size. The mean particle size calculated of commercial Pt/C was ~1.6 nm, while for $Pt_{0.50}$–$(CeO_2)_{0.50}$/C and $Pt_{0.50}$–$(RuO_y)_{0.50}$/C, this was 2.1 and 2.2 nm, respectively, although a few large agglomerates (~6.0 nm) were observed for the $Pt_{0.50}$–$(CeO_2)_{0.50}$/C composite. A similar slight increase in particle size was also observed for the ternary composite catalysts, where mean particle sizes of 2.5, 2.1, and 2.1 nm were observed for the $Pt_{0.25}$–$(RuO_y$–$CeO_2)_{0.75}$/C, $Pt_{0.50}$–$(RuO_y$–$CeO_2)_{0.50}$/C, $Pt_{0.75}$–$(RuO_y$–$CeO_2)_{0.25}$/C composites, respectively (Fig. 2). The highest co-catalyst addition (75 %) resulted in a small number (less than 0.9 %) of large agglomerates, probably due to the aggregation of co-catalyst nanoparticles.

The metal atomic ratio of the different catalysts, determined by ICP-OES, were the follows: 25.2:74.8 for $Pt_{0.25}$–$(RuO_y$–$Ce)_{0.75}$/C, 50.6:49.4 for $Pt_{0.50}$–$(RuO_y$–$CeO_2)_{0.50}$/C and 73.9:26.1 for $Pt_{0.75}$–$(RuO_y$–$CeO_2)_{0.25}$/C, demonstrating a good agreement between the experimental and the expected theoretical values, as already reported for catalysts synthesized by sol–gel method [18, 31].

Figure 3a, b shows cyclic voltammograms obtained at 100 mV s^{-1} for the $Pt_{0.50}$–$(CeO_2)_{0.50}$/C and $Pt_{0.50}$–$(RuO_y)_{0.50}$/C binary composites compared with commercial Pt/C and for $Pt_{0.25}$–$(RuO_y$–$CeO_2)_{0.75}$/C, $Pt_{0.50}$–$(RuO_y$–$CeO_2)_{0.50}$/C, and $Pt_{0.75}$–$(RuO_y$–$CeO_2)_{0.25}$/C, respectively. The curves show typical behaviour regarding the hydrogen adsorption/desorption and Pt oxide regions in the catalysts when H_2SO_4 0.5 mol L^{-1} solutions were used. However, the different co-catalysts for Pt inhibited these features, mainly for the ternary composites. Thus, the addition of Ru and Ce in the ternary catalytic composites decreased the processes of adsorption/desorption of hydrogen, which are typical of a polycrystalline Pt surface. In fact, the higher the co-catalyst amount, the lower the current in the adsorption/desorption of hydrogen region, suggesting alloy formation as observed by XRD, or possibly the deposition of Ru and/or Ce on the Pt surface, diminishing its exposed superficial area.

It is also important from the catalytic point of view that the electrochemically exposed surface area of the ternary catalysts prepared in this study was not significantly different (Fig. 3b), which is in agreement with the small differences in the particle size distribution and mean particle size of the catalysts observed by TEM (Fig. 2).

3.2 Electrochemical catalysis behaviour towards the oxidation of ethanol

Chronoamperometric experiments were recorded for 600 s at 600 mV versus HESS to compare the catalytic activities of the prepared catalysts under steady-state conditions. The steady-state behaviour of the catalyst may be different from the potentiodynamic behaviour, due to differences in both the reaction and diffusion rates. Figure 4a, b shows the transient currents for ethanol electro-oxidation on commercial Pt/C and Pt–Ru/C, and on the $Pt_{0.50}$–$(CeO_2)_{0.50}$/C and $Pt_{0.50}$–$(RuO_y)_{0.50}$/C binary composites and for the $Pt_{0.25}$–$(RuO_y$–$CeO_2)_{0.75}$/C, $Pt_{0.50}$–$(RuO_y$–$CeO_2)_{0.50}$/C, and $Pt_{0.75}$–$(RuO_y$–$CeO_2)_{0.25}$/C ternary composites, respectively. Just after the initial step potential, the faradaic current fell very rapidly due to the double layer charging and other fast processes at the electrode surface. This was followed by a slow change towards a quasi-steady state after the first 5 min.

The final pseudo-current density taken at the $Pt_{0.50}$–$(RuO_y)_{0.50}$/C composite was almost two-fold higher than the one taken at the Pt–Ru/C commercial composite and approximately threefold higher than that observed at Pt/C (Fig. 4a). In this context, the electrocatalytic activity for methanol electro-oxidation at PtRu catalyst rich in amorphous hydrous ruthenium oxide was found to be two orders of magnitude higher, in terms of exchange current density, than its reduced (Pt^0Ru^0) counterpart catalyst [28]. The superior performance of the amorphous ruthenium oxide-rich PtRu catalysts was attributed to the uniqueness of this material as a mixed electron/proton conductor, innately related to Ru–OH speciation [28]. The highly beneficial effect of amorphous ruthenium oxide in the PtRu catalyst on methanol electro-oxidation was thereafter frequently confirmed experimentally in different laboratories [28–31]. Amorphous hydrous ruthenium oxide acts as an efficient promoter of Pt for the electro-

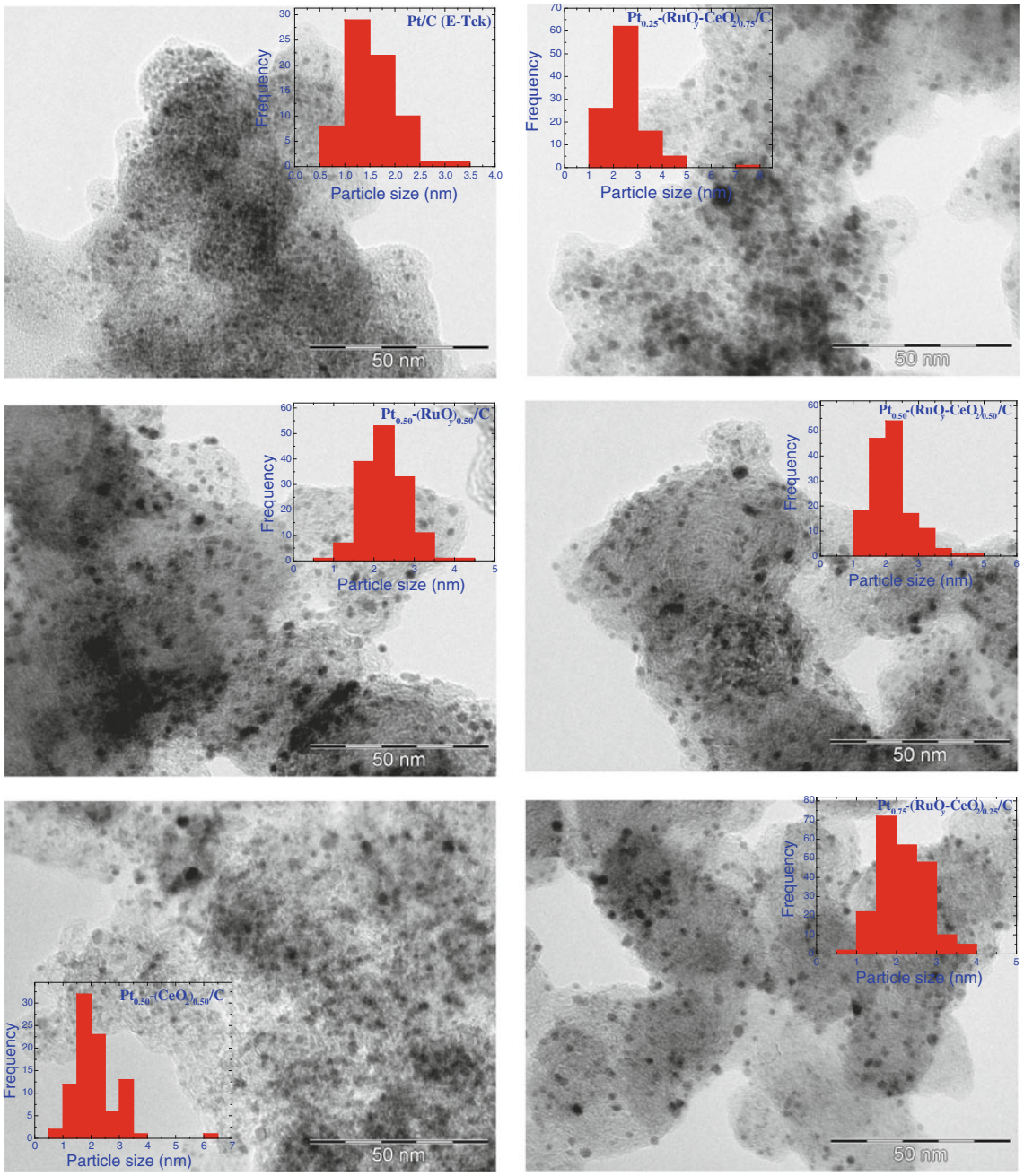

Fig. 2 TEM images and histograms of the particle-size distribution obtained for the Pt/C (E-Tek), $Pt_{0.50}$–$(RuO_y)_{0.50}$/C, $Pt_{0.50}$–$(CeO_2)_{0.50}$/C, $Pt_{0.25}$–$(RuO_y$–$CeO_2)_{0.75}$/C, $Pt_{0.50}$–$(RuO_y$–$CeO_2)_{0.50}$/C, and $Pt_{0.75}$–$(RuO_y$–$CeO_2)_{0.25}$/C catalysts

oxidation of CO and methanol [32]. This enhanced catalytic activity may be due to a modified bifunctional mechanism, when the required water molecule for the complete oxidation reaction does not necessarily have to come directly from the electrolyte solution, but can also come from the structure of amorphous hydrous ruthenium oxide. Although studies using both Pt and amorphous ruthenium oxides for the ethanol oxidation reaction are very scarce, the beneficial effect of these oxides in the electro-oxidation of methanol and mainly of CO could be vital for the ethanol oxidation and its reaction intermediaries, as observed in our study.

The pseudo-current density initially decreased but recovered after the first 10–20 s at the $Pt_{0.50}$–$(CeO_2)_{0.50}$/C composite, probably due to the oxidation of ethanol oxidation reaction intermediaries formed in the initial stages of the reaction. After ~250 s, the current had values higher than that observed for Pt/C, suggesting a slight beneficial effect of the presence of co-catalysts. In this context, De Souza et al. [22], using cyclic voltammetry and

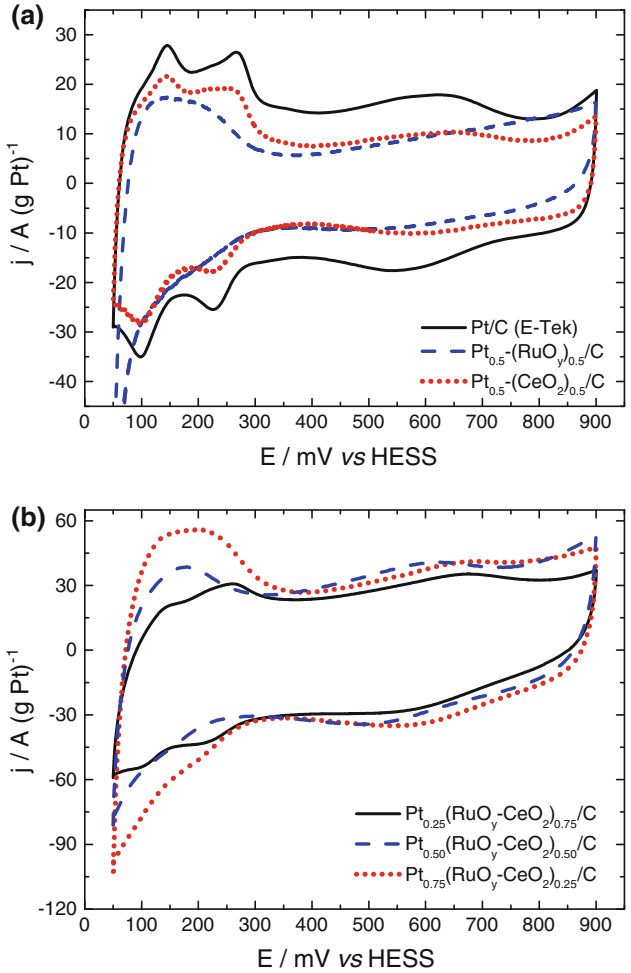

Fig. 3 Cyclic voltammetric plots (second cycle) for the Pt/C E-Tek, $Pt_{0.50}$–$(CeO_2)_{0.50}$/C, and $Pt_{0.50}$–$(RuO_y)_{0.50}$/C (**a**) and $Pt_{0.25}$–$(RuO_y$–$Ce)_{0.75}$/C, $Pt_{0.50}$–$(RuO_y$–$CeO_2)_{0.50}$/C, and $Pt_{0.75}$–$(RuO_y$–$CeO_2)_{0.25}$/C (**b**) electrocatalytic composites in 0.5 mol L^{-1} H_2SO_4 support electrolyte at 100 mV s^{-1}. All composites were deposited on a BDD electrode

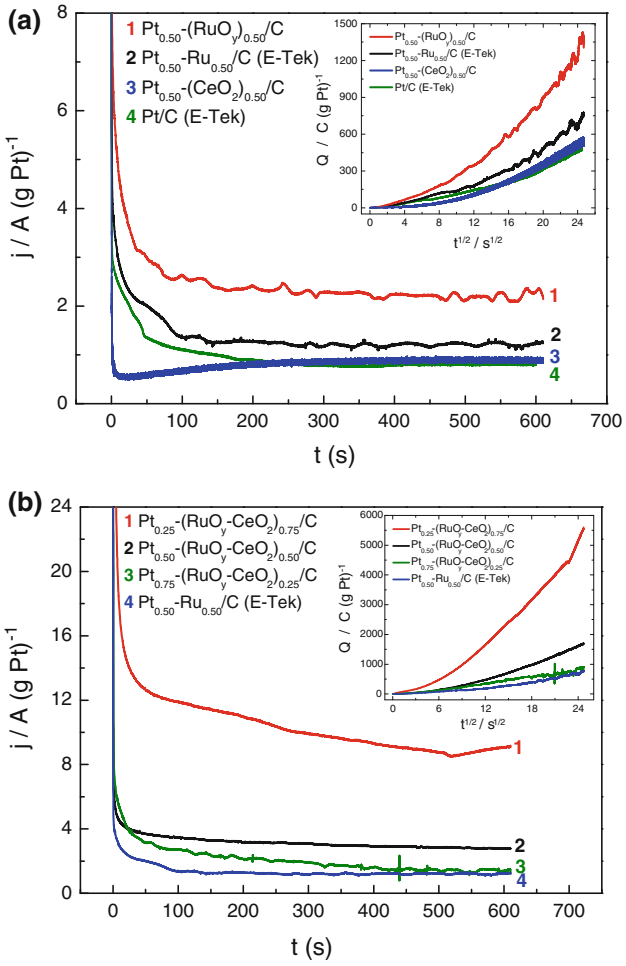

Fig. 4 Chronoamperometric curves for the oxidation of ethanol on the **a** Pt/C, $Pt_{0.50}$–$Ru_{0.50}$/C (both E-Tek), $Pt_{0.50}$–$(CeO_2)_{0.50}$/C, $Pt_{0.50}$–$(RuO_y)_{0.50}$/C. **b** $Pt_{0.25}$–$(RuO_y$–$CeO_2)_{0.75}$/C, $Pt_{0.50}$–$(RuO_y$–$CeO_2)_{0.50}$/C, and $Pt_{0.75}$–$(RuO_y$–$CeO_2)_{0.25}$/C composites in 0.5 mol L^{-1} C_2H_5OH + 0.5 mol L^{-1} H_2SO_4 solution. *Inset* charge density versus $t^{1/2}$ plots of the studied catalysts from chronoamperometric curves

chronoamperometry, showed that Pt–CeO_2/C (1:3, atomic ratio) has higher ethanol electro-oxidation activity compared to both the Pt/C and Pt–Ru/C (E-Tek) materials. The higher catalytic activity was attributed to several intrinsic features, including reduced poisoning by the strongly bound intermediates.

The catalytic activity was improved on the ternary catalytic composites. $Pt_{0.25}$–$(RuO_y$–$CeO_2)_{0.75}$/C yielded the highest steady-state pseudo-current density. The Ru atoms favour CO–O coupling and also the oxidation of other adsorbed intermediates by providing oxygen species and producing higher electrochemical currents, while Ce oxide acts by weakening CO adsorption and providing superficial oxides to promote the oxidation process and the consequent oxidation of the strongly bound intermediates [33]. Moreover, the activity of the $Pt_{0.25}$–$(RuO_y$–$CeO_2)_{0.75}$/C/BDD and $Pt_{0.50}$–$(RuO_y$–$CeO_2)_{0.50}$/C/BDD electrodes was higher when compared to Pt/C, suggesting the participation of Ru and Ce in a multi-functional effect.

The Pt–Ru/C electrode showed rapid current density decay and very low initial and final current densities. This indicates that the Pt–Ru/C surface is prone to poisoning by ethanolic residues. Current density decay was comparatively low for the $Pt_{0.25}$–$(RuO_y$–$CeO_2)_{0.75}$/C catalytic composite. Nevertheless, high initial as well as final current densities were observed. Thus, the $Pt_{0.25}$–$(RuO_y$–$CeO_2)_{0.75}$/C catalysts demonstrated greater tolerance to ethanolic residues.

The Anson's plots (following Eq. 1) [34] shown in the inset of Fig. 4a, b allows the determination of the amount of charge involved in the electrochemical process for the different electro-catalysts under investigation. These curves demonstrate a high level of charge on the ternary

electrodes, mainly for $Pt_{0.25}$–$(RuO_y$–$CeO_2)_{0.75}$/C/BDD, that was much higher than both that produced by Pt–Ru/C/BDD (E-Tek) (~7.3-fold) and that produced by Pt/C/BDD (~11.7-fold), as shown in Fig. 4a. The fact that ~5,600 C is generated per g Pt at the ternary catalyst in 600 s of experiment compared with only 480 C generated per g Pt at Pt/C catalyst is significant from the practical point of view.

$$Q = \frac{2nFAcD^{1/2}}{\pi^{1/2}} t^{1/2} \quad (1)$$

where c is the concentration of electroactive specie, A is the apparent electrode surface area, D is the diffusion coefficient and other symbols are as usual.

We estimated the long-term poisoning rates (δ) by measuring the linear decay of the current at times greater than 200 s in the chronoamperometric curves from Fig. 4, using a procedure described in literature [35] (Eq. 2). The long-term poisoning effect for ethanol oxidation was 0.045 % s^{-1} for the $Pt_{0.25}$–$(RuO_y$–$CeO_2)_{0.75}$/C and for $Pt_{0.50}$–$(RuO_y$–$CeO_2)_{0.50}$/C catalysts while it was higher at Pt/C (0.079 % s^{-1}). Since on metals of the Pt group the ethanol oxidation reaction proceed through the formation of reactive intermediates (like CH_3CO_{ads}) and the ultimate poisoning species (CO_{ads}) [36], it appears that the reaction, in its course, follows a different pathway on the Pt catalyst and on the ternary catalysts. This assertion will be discussed hereafter.

$$\delta = -\frac{100}{j_{t=0}} \left(\frac{dj}{dt}\right)_{t>200} \quad (2)$$

Cyclic voltammetry measurements at room temperature also compared the electrocatalytic activities for the oxidation of ethanol of the different catalysts. In Fig. 5a, the catalytic activity of the binary composites is higher when compared to that on Pt/C (E-Tek), since in the binary composites, the pseudo-current density values were higher at high potentials with pseudo-current density peak values in the forward scan (j_F) of about 64, 104, and 133 at Pt/C, $Pt_{0.50}$–$(RuO_y)_{0.50}$/C and $Pt_{0.50}$–$(CeO_2)_{0.50}$/C, respectively, with an emphasis on the ceria-containing catalyst. This suggests a higher amount of ethanol being oxidized in the forward scan. The onset potential of the ethanol oxidation reaction also occurred at lower potential values at the binary composites, mainly for the $Pt_{0.50}$–$(RuO_y)_{0.50}$/C/BDD electrode (inset of Fig. 5a). In addition, the ratio between the pseudo-current density peaks in the forward and backward direction scans (j_F/j_B) was higher at the $Pt_{0.50}$–$(RuO_y)_{0.50}$/C/BDD electrode (1.37) than at the Pt/C/BDD and $Pt_{0.50}$–$(CeO_2)_{0.50}$/C/BDD electrodes (0.95 and 0.68, respectively), suggesting less poisoning in the catalyst containing ruthenium.

Given that the co-catalyst present in Pt/C showed synergistic behaviour in the ethanol oxidation reaction, their combination should also produce enhanced catalytic activity towards this alcohol oxidation, as already observed by chronoamperometry (Fig. 4).

Thus, cyclic voltammetry measurements for the ethanol oxidation in acid media were carried out at the ternary catalyst prepared in this study and at a Pt–Ru/C commercial catalyst (Fig. 5b). The voltammetric curves show similar electrocatalytic activity at low over-potentials, but at high over-potentials, the materials containing both Ru and Ce demonstrated superior performance in comparison with the Pt–Ru/C/BDD electrode. The onset potentials of ethanol oxidation (determined using a fixed pseudo-current density of 10 A $(g\ Pt)^{-1}$) were 544, 462, 440, and 365 mV at the Pt–Ru/C, $Pt_{0.75}$–$(RuO_y$–$CeO_2)_{0.25}$/C, $Pt_{0.50}$–$(RuO_y$–$CeO_2)_{0.50}$/C, and $Pt_{0.25}$–$(RuO_y$–$CeO_2)_{0.75}$/C catalysts, respectively. The double layer current was subtracted in each voltammogram to determine the onset reaction potentials in the voltammograms (figure not shown). Owing to the low onset potential values observed for the ternary catalysts with a high amount of Ru and Ce, the pseudo-current density, taken at 1000 mV, increased by ~910 % at the $Pt_{0.25}(RuO_y$–$CeO_2)_{0.75}$/C composite when compared with Pt/C (Fig. 5a) and ~305 % versus Pt–Ru/C in Fig. 5b.

The j_F/j_B ratio evaluates catalyst tolerance to the accumulation of carbonaceous species [37, 38]. Lower ratio values imply high surface coverage by reaction intermediary species and low efficiency towards alcohol oxidation. Consequently, the j_F/j_B ratio is a very useful parameter to evaluate the influence of the addition of different co-catalysts in Pt-based catalysts on the electro-oxidation of ethanol. The j_F/j_B ratios of some of the studied catalysts (Fig. 5c) increased in the order: Pt/C, Pt–Ru/C, $Pt_{0.75}$–$(RuO_y$–$CeO_2)_{0.25}$/C, $Pt_{0.50}$–$(RuO_y$–$CeO_2)_{0.50}$/C, and $Pt_{0.25}$–$(RuO_y$–$CeO_2)_{0.75}$/C. The inset of Fig. 5c shows that the relationship between the j_F and j_B was almost linear with both the addition of Ru and $(RuO_y$–$CeO_2)$ co-catalysts, and with the amount of co-catalyst for the ternary composites. Thus, while Pt/C underwent severe catalyst poisoning, the synergistic effect of the $(RuO_y$–$CeO_2)$ co-catalyst addition suggests low surface poisoning. These voltammetric analyses agree perfectly with the low long-term poisoning effect for ethanol oxidation calculated for the $Pt_{0.25}$–$(RuO_y$–$CeO_2)_{0.75}$/C and $Pt_{0.50}$–$(RuO_y$–$CeO_2)_{0.50}$/C catalysts on the chronoamperometric curves in Fig. 4 (i.e., 0.045 % s^{-1} for both catalysts) in contrast with the higher poisoning effect determined for Pt/C (0.079 % s^{-1}). It confirms the importance of the use of RuO_y–CeO_2 as co-catalyst to Pt.

The use of the derivative voltammetry technique for the evaluation of methanol oxidation reaction activities of different electro-catalysts was recently demonstrated in the

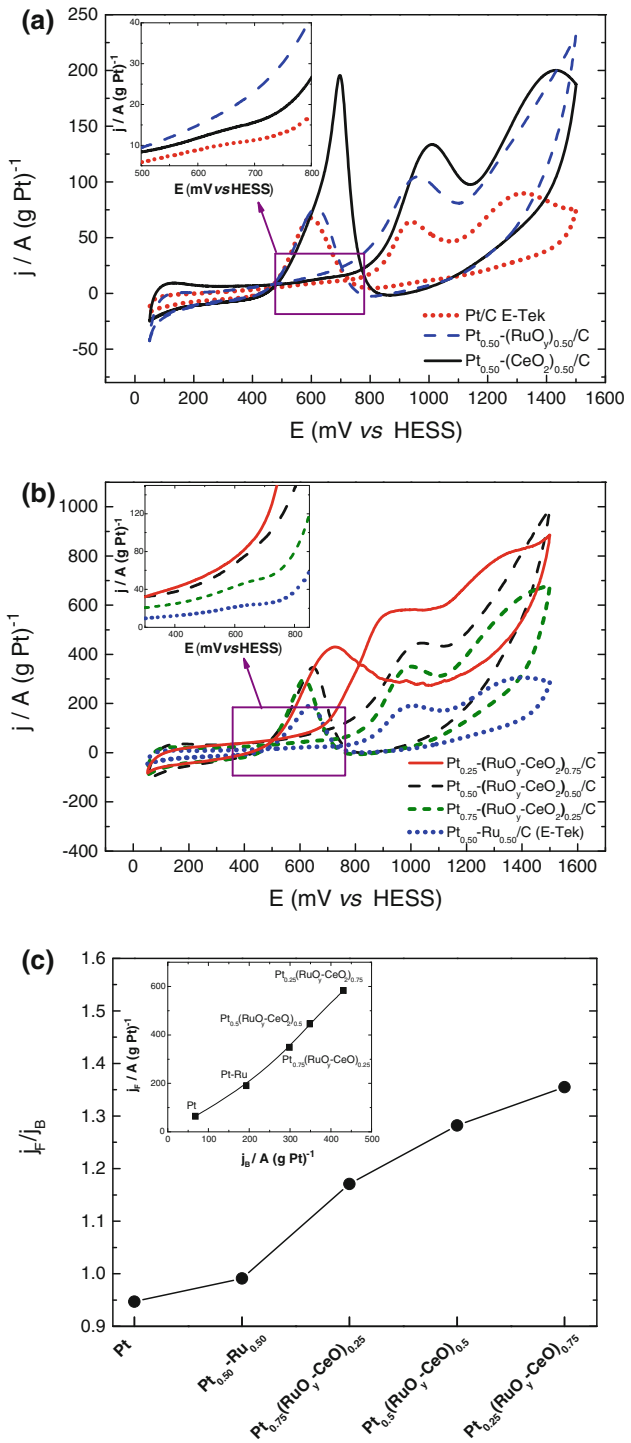

Fig. 5 Cyclic voltammograms for ethanol oxidation at the **a** Pt/C, $Pt_{0.50}$–$(CeO_2)_{0.50}$/C, $Pt_{0.50}$–$(RuO_y)_{0.50}$/C. **b** $Pt_{0.25}$–$(RuO_y$–$CeO_2)_{0.75}$/C, $Pt_{0.50}$–$(RuO_y$–$CeO_2)_{0.50}$/C, and $Pt_{0.75}$–$(RuO_y$–$CeO_2)_{0.25}$/C composites in 0.5 mol L^{-1} C_2H_5OH + 0.5 mol L^{-1} H_2SO_4 solution. Scan rate of 50 mV s^{-1}. Magnified views of the onset regions of cyclic voltammograms. **c** Variation in the forward and backward peak pseudo-current density ratio (j_F/j_B) and forward peak pseudo-current density (j_F) versus backward peak pseudo-current density (j_B) plots (*inset*) for the electro-oxidation of ethanol on some studied catalysts

literature [39]. The derivative technique has a better signal-to-noise ratio, accuracy of locating the voltammetric peak potential and onset potential of alcohol and manifests important mechanistic features for alcohol oxidation.

Various surface reactions that control the voltammetric current can be better understood by derivative voltammograms [40] that have more voltammetric features than normal voltammograms. Figure 6 delineates the first derivative voltammograms (thick black curves) and their normal linear voltammograms (thin red curves) for the oxidation of ethanol at the Pt/C, Pt–Ru/C and $Pt_{0.25}$–$(RuO_y$–$CeO_2)_{0.75}$/C catalytic composites.

The derivative voltammogram represents the rate of change of voltammetric current I with respect to electrode potential E (dI/dE). For the Pt/C catalyst, the derivative voltammogram of Fig. 6 can be related to some mechanistic insight as follows: at low potentials (from point a to point b), dissociative adsorption of ethanol occurs and with subsequent removal of hydrogen atoms from the molecule (dissociation of C–H), several parallel reactions can also occur at this low potential with the production of various adsorbed compounds, like acetyl and acetate (without C–C bond cleavage), or CO and methyl resulting from C–C bond cleavage [41]. Most of the Pt active surface sites are then covered with adsorbed reaction intermediaries.

The voltammetric current, as well as dI/dE, were nearly zero up to ~0.70 V (point b), and ethanol oxidative dissociation can be considered as the rate-determining step at lower potentials for the Pt/C and Pt–Ru/C composites (Fig. 6). However, it is clear from Fig. 6 that this region is short for the ternary catalyst and that point b is around 0.42 V, i.e. 0.28 V more negative. Note that, this shift to more negative potentials at the ternary composite compared to Pt–Ru/C was also observed in the cyclic voltammograms in Fig. 5c.

From point b to point c, and due to the increase in potential, the adsorbed reaction intermediaries (mainly CO and CH_3) are oxidized to CO_2 or, to a lesser degree, the adsorbed acetyl and acetate react to form free acetic acid by two different pathways, freeing more sites to continue the reaction. Thus, the dI/dE value increases in this region.

Although the shape of the derivative voltammogram taken for Pt–Ru/C is very similar to the Pt/C, both the dI/dE values (black curve) and the current (red curve) in this region (point c) are higher at Pt–Ru/C, indicating a larger catalytic surface. For Pt–Ru, CO oxidation occurs at lower potential due to a bifunctional mechanism (oxidation by OH adsorbed on the Ru islands) or a ligand effect (oxidation by OH formed on Pt atoms near the Ru islands and weakening of the Pt–CO bond), enabling a reaction with the OH group at lower potentials [42, 43]. Since the shape

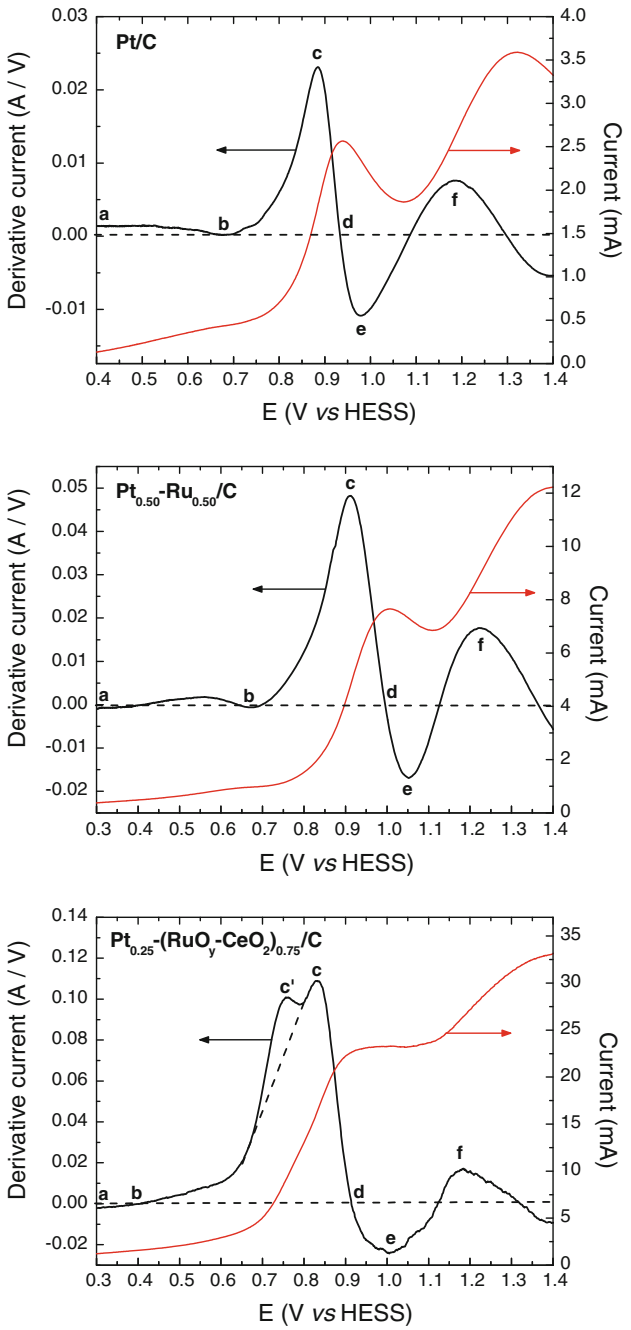

Fig. 6 Anodic scans of cyclic (*right axes*) and derivative (*left axes*) voltammograms of the ethanol oxidation reaction at Pt/C/BDD, $Pt_{0.50}$–$Ru_{0.50}$/C/BDD, and $Pt_{0.25}$–$(RuO_y$–$CeO_2)_{0.75}$/C/BDD in 0.5 mol L^{-1} H_2SO_4 + 0.5 mol L^{-1} ethanol at 50 mV s^{-1}, showing the various potential regions and mechanistic aspect of ethanol oxidation

of these derivative voltammograms is similar, then the oxidation mechanism must be also similar, only increased in magnitude by the presence of Ru, since at potentials from ~0.8 V, Pt is able to produce OH species like Ru does at lower potentials.

A further increase in the potential results in the generation of more OH on Pt sites, which tends to block ethanol adsorption and its consequent oxidation. The above process is pointed out by a decrease in the d*I*/d*E* values from point c to point e. The oxidative removal of OH_{ads} may be thought of as the rate-determining step in this stage. At point d, the d*I*/d*E* value reaches zero, at which point the voltammetric current reaches a maximum and then starts decreasing. The d*I*/d*E* values become negative after point d because the beneficial effect of OH_{ads} is now unfavourable as OH species are strongly adsorbed to Pt sites, blocking ethanol adsorption from the bulk solution. d*I*/d*E* reaches its lowest value at point e, where the active sites of the catalyst are almost covered by OH_{ads}.

The second peak in the normal voltammetry curves of Fig. 5 is ascribed to both the oxidation of ethanol to acetic acid from adsorbed acetyl and to the oxidation of acetic acid to CO_2, depending on the reaction pathway [41, 44]. Thus, the increase in the d*I*/d*E* values from point e to point f may be related to the reaction of already adsorbed species on the catalyst surface to form acetic acid and/or the oxidation of acetic acid to CO_2. Ethanol oxidation reaction selectivity is shifted towards the production of acetic acid [45] with increasing Ru content [46]. This suggests that the bifunctional mechanism (enabling the reaction of the C intermediate with OH) and the ligand effect (weakening of the Pt–C adsorbate intermediate bond) could both be responsible for the performance enhancement in direct ethanol fuel cells. In addition, the preferential reaction pathway on the Pt (111) surface is the reaction to form acetate and acetic acid [47]. These observations agree with the high peaks in the derivative voltammograms of Pt/C and Pt–Ru/C at point f, mainly due to the formation of undesirable acetic acid; thus, their use must be avoided in practical applications.

From point f, the derivative signals decay, probably due to covering of the Pt surface with oxides, hindering further ethanol oxidation.

On the other hand, the derivative voltammogram of the $Pt_{0.25}$–$(RuO_y$–$CeO_2)_{0.75}$/C composite has a different shape than that of Pt and Pt–Ru catalysts. A new peak designated point c' appeared, representing a change in the oxidation mechanism or the emergence of a new parallel reaction pathway. Note that the size of the ratio of both peaks at points f/c in the derivative voltammogram and of the peak in the normal voltammogram at higher potentials (from ~1.2 to 1.4 V), related to the peak at around 0.9–1.0 V, are lower in the ternary catalyst when compared with the ratios observed at Pt and Pt–Ru. Thus, if the peak at higher potentials is ascribed mainly to complete acetic acid oxidation previously formed through the pathway that formed adsorbed acetyl and acetate, this is a minor pathway at the ternary catalyst. Hence, the new peak at point c' could be related to the direct oxidation of ethanol to CO_2 via the pathway that formed CO and CH_3 (with the cleavage of the

C–C bond) that are oxidized to CO_2 aided by the functional mechanism present at both RuO_y (improved because hydrous ruthenium oxide formed at the electrode surface in solution is a mixed proton and electron conductor and innately expresses Ru–OH speciation) [28] and at CeO_2, reactions (1), (2), and (3) occur [40].

Ceria is capable of storing and releasing oxygen with a reversible transition between the +4 and +3 oxidation states:

$$CeO_2 \rightleftharpoons CeO_{2-x} + (x/2)O_2 \quad (3)$$

where $(0 \leq x \leq 0.5)$

$$CeO_{2-x} + H_2O \rightarrow CeO_{2-x} - (OH) + H^+ + e^- \quad (4)$$

$$Pt - CO + CeO_{2-x} - (OH) \rightarrow Pt + CeO_{2-x} + CO_2 + H^+ + e^- \quad (5)$$

Furthermore, it is known that the oxygen vacancies in CeO_{2-x} may provide active sites for CO adsorption, with the consequent liberation of more Pt sites for further oxidation reactions [40].

Note that without the presence of the peak at point c' in the derivative voltammogram of the ternary composite, the curve must follow the dashed line in the figure and the shape of the curve will be similar to that observed for the other catalysts, following the pathways without C–C cleavage at low potentials, and leading to the production of high amounts of acetic acid.

Steady-state polarization curves are very useful tools for the study of the electrochemical oxidation of ethanol, mainly when the corresponding Tafel plots are used, since these furnish a direct comparison of onset potentials and electrochemical activities in a straightforward manner. Figure 7 shows the Tafel plots taken for the commercial Pt/C and Pt–Ru/C catalysts, and on the $Pt_{0.25}$–$(RuO_y$–$CeO_2)_{0.75}$/C, $Pt_{0.50}$–$(RuO_y$–$CeO_2)_{0.50}$/C, and $Pt_{0.75}$–$(RuO_y$–$CeO_2)_{0.25}$/C ternary composites, all having good linearity (R^2 in the range of 0.99340–0.99855). Data were obtained in potentiostatic mode after 300 s of polarization at each potential. The best catalytic activity for ethanol oxidation was obtained for the catalyst containing (RuO_y–CeO_2) in the highest amount (75 %).

The Tafel plots in Fig. 7 indicate that the ethanol oxidation process starts at 530, 411, 400, 360, and 333 mV versus HESS on the Pt/C/BDD, Pt–Ru/C/BDD, $Pt_{0.75}$–$(RuO_y$–$CeO_2)_{0.25}$/C/BDD, $Pt_{0.50}$–$(RuO_y$–$CeO_2)_{0.50}$/C/BDD, and $Pt_{0.25}$–$(RuO_y$–$CeO_2)_{0.75}$/C/BDD electrodes, respectively (Table 2). The addition of a high amount (75 %) of (RuO_y–CeO_2) to Pt/C produces a very active electrocatalyst, lowering the onset potential by ~197 mV. It is worth mentioning that the observed onset potential on the Pt/C/BDD electrode (530 V) is in agreement with those reported in the literature [38] for this electrode and for Pt

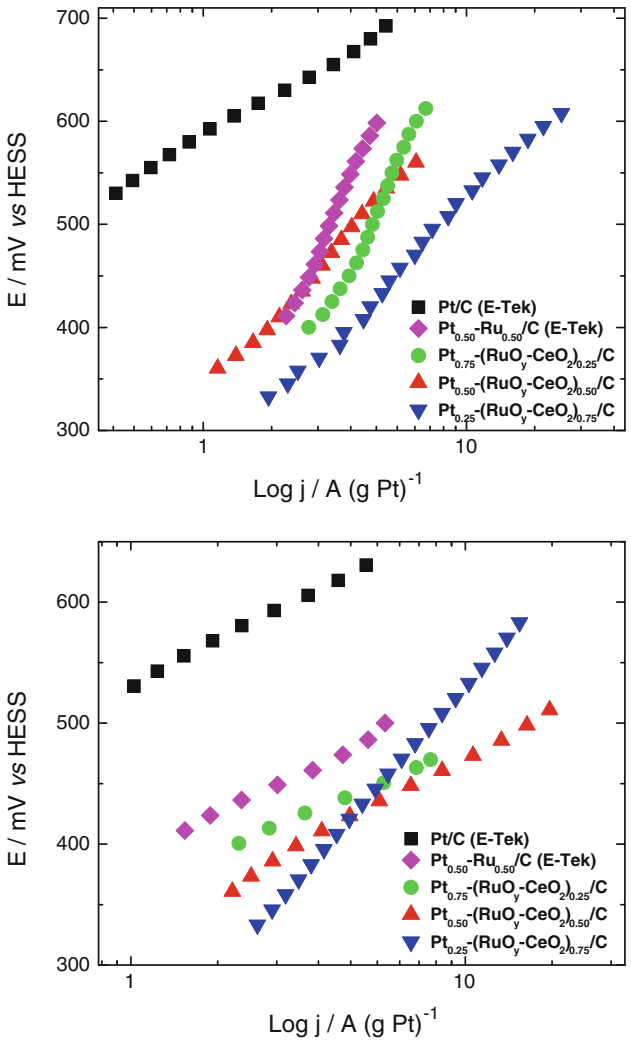

Fig. 7 Tafel plots for 0.5 mol L^{-1} ethanol electrochemical oxidation in acid medium (0.5 mol L^{-1} H_2SO_4) obtained at the Pt/C, $Pt_{0.50}$–$Ru_{0.50}$/C, $Pt_{0.25}$–$(RuO_y$–$CeO_2)_{0.75}$/C, $Pt_{0.50}$–$(RuO_y$–$CeO_2)_{0.50}$/C, and $Pt_{0.75}$–$(RuO_y$–$CeO_2)_{0.25}$/C catalytic composites. All data were obtained based on the values of the potentiostatic current measured after 300 s of polarization every 20 mV

directly deposited on BDD [24]. For the $Pt_{0.25}$–$(RuO_y$–$CeO_2)_{0.75}$/C ternary composite catalysts (Fig. 7), improved performance was also observed due to an increase in the pseudo-current density measured at 530 mV of nearly threefold compared to the value obtained for the commercial Pt–Ru/C catalyst and about 23-fold when compared with Pt/C (Table 2).

The Tafel slopes displayed in Table 2 strongly suggest that the ethanol oxidation reaction at Pt/C and at $Pt_{0.25}$–$(RuO_y$–$CeO_2)_{0.75}$/C occurs via different reaction mechanisms, as already demonstrated by derivative voltammetry (Fig. 6). The Tafel slope taken for Pt/C (139 mV dec^{-1}) is near the values observed over a polycrystalline Pt electrode [48] and Pt supported on glassy carbon [49] (120–132 mV dec^{-1}), but in alkaline media. The Tafel slope for $Pt_{0.50}$–$(RuO_y)_{0.50}$/C and

Table 2 Onset potential of the ethanol electro-oxidation reaction, pseudo-density of the current measured at 530 mV versus HESS and Tafel slope values; all data from Tafel plots (Fig. 7)

Catalytic composite	Reaction onset potential/V vs. HESS	Pseudo-current density measured at 530 mV/A (g Pt)$^{-1}$	Tafel slope/ mV dec^{-1}
Pt/C (E-Tek)	530	0.46	139
$Pt_{0.50}$–$Ru_{0.50}$/C (E-Tek)	411	3.33	130
$Pt_{0.50}$–$(RuO_y)_{0.50}$/C	460	2.81	331
$Pt_{0.50}$–$(CeO_2)_{0.50}$/C	504	1.13	124
$Pt_{0.75}$–$(RuO_y$–$CeO_2)_{0.25}$/C	400	4.83	111
$Pt_{0.50}$–$(RuO_y$–$CeO_2)_{0.50}$/C	360	4.84	155
$Pt_{0.25}$–$(RuO_y$–$CeO_2)_{0.75}$/C	333	10.61	329

$Pt_{0.50}$–$(CeO_2)_{0.50}$/C were 331 and 124 mV dec^{-1}, respectively, also suggesting different reaction mechanisms. Note that the Tafel slope for the commercial $Pt_{0.50}$–$Ru_{0.50}$/C was 130 dec^{-1}, suggesting that the presence of ruthenium oxides in the catalyst modifies the rate determining step of the reaction. The Tafel slopes for the ternary catalysts with the higher co-catalyst content were in the range of 155–329 mV dec^{-1}, showing that the higher the ruthenium and cerium oxides content in the catalyst the higher the Tafel slope probably due to the contribution of ruthenium oxides, like in the binary catalyst $Pt_{0.50}$–$(RuO_y)_{0.50}$/C; however, the ethanol oxidation mechanism is extremely complex and still requires further experimental evidence to allow for the establishment of the rate determining step, thus allowing theoretical calculations of the Tafel slope value (b).

Note that since the particle size of the binary and ternary composites was in a wide range (2.1–2.5 nm), the performance of the composites obtained by the sol–gel method is mainly dependent on the catalytic activity and not a size effect of the particle, as previously reported by our research group [18, 50]. The support for this statement is observed in the particle-size distributions of Fig. 2, where the particle sizes of all catalysts vary randomly between 2.1 and 2.5 nm and do not present a tendency that agrees with the catalytic activity observed in the experiments of cyclic and derivative voltammetry, chronoamperometry and the Tafel plots discussed until this point.

4 Conclusions

This study describes the superior catalytic activity towards ethanol oxidation of ternary Pt_x–$(RuO_y$–$CeO_2)_{1-x}$/C catalytic composites ($x = 0.25$, 0.50, or 0.75), prepared by the sol–gel method. XRD measurements demonstrated the successful deposition of the co-catalysts on Pt/C as cerium oxide (CeO_2) and as an alloy between Ru and Pt; however, a previous study also demonstrated the presence of amorphous Ru oxides (thus designated RuO_y, where $y = 0$, +2, or +6). The small size of the synthesized nanoparticles (2.1–2.5 nm in diameter) confirmed that the relatively simple and low-cost sol–gel method is a very useful technique to prepare nanoparticulate catalysts, as already shown [18, 24, 31, 50].

Different electrochemical experiments showed that the addition of high amounts of co-catalysts (50–75 %) to Pt led to enhanced catalytic activity towards the electro-oxidation of ethanol in acid media, mainly for the $Pt_{0.25}$–$(RuO_y$–$CeO_2)_{0.75}$/C catalytic composite, which presented outstanding catalytic activity. Derivative voltammetry and Tafel plots demonstrated that the superior catalytic activity of this ternary catalyst is related to a change in the reaction mechanism, where the pathway that formed CO and CH_3 (with cleavage of the C–C bond), which are further oxidized to CO_2, was aided by the bifunctional mechanism present at both RuO_y and CeO_2.

Thus, $Pt_{0.25}$–$(RuO_y$–$CeO_2)_{0.75}$/C/BDD electrodes showed high catalytic activity towards ethanol oxidation. This justifies further research to better understand the role of the studied co-catalyst in the reaction mechanism and the intermediary products of the reaction when used as catalysts in anode electrodes.

Acknowledgments The authors thank the National Council of Technological and Scientific Development-CNPq of Brazil (Grants 304018/2009-0 and 481788/2010-7) for the scholarships and financial support for this study.

References

1. Wang Z-B, Yin G-P, Shao Y-Y, Yang B-Q, Shi P-F, Feng P-X (2007) Electrochemical impedance studies on carbon supported PtRuNi and PtRu anode catalysts in acid medium for direct methanol fuel cell. J Power Sources 165:9
2. Wang Y, Chen KS, Mishler J, Cho SC, Adroher XC (2011) A review of polymer electrolyte membrane fuel cells: technology, applications, and needs on fundamental research. Appl Energ 88:981
3. Sharma S, Pollet BG (2012) Support materials for PEMFC and DMFC electrocatalysts—a review. J Power Sources 208:96
4. Peighambardoust SJ, Rowshanzamir S, Amjadi M (2010) Review of the proton exchange membranes for fuel cell applications. Int J Hydrogen Energ 35:9349

5. Andújar JM, Segura F (2009) Fuel cells: history and updating. A walk along two centuries. Renew Sust Energ Rev 13:2309
6. Oliveira RTS, Santos MC, Marcussi BG, Nascente PAP, Bulhões LOS, Pereira EC (2005) The use of a metallic bilayer for the oxidation of small organic molecules. J Electroanal Chem 575:177
7. Wan C-H, Lin M-T (2013) Mitigating methanol crossover with self-assembled Pt_{35}–Ru_{65} catalyst on Nafion surface. J Power Sources 222:470
8. Léger J-M, Rousseau S, Coutanceau C, Hahn F, Lamy C (2005) How bimetallic electrocatalysts does work for reactions involved in fuel cells? Example of ethanol oxidation and comparison to methanol. Electrochim Acta 50:5118
9. Wu J, Yuan XZ, Martin JJ, Wang H, Zhang J, Shen J, Wu S, Merida W (2008) A review of PEM fuel cell durability: degradation mechanisms and mitigation strategies. J Power Sources 184:104
10. Lima FHB, Profeti D, Chatenet M, Riello D, Ticianelli EA, Gonzalez ER (2010) Electro-oxidation of ethanol on Rh/Pt and Ru/Rh/Pt sub-monolayers deposited on Au/C nanoparticles. Electrocatal 1:72
11. Koponen U, Kumpulainen H, Bergelin M, Keskinen J, Peltonen T, Valkiainen M, Wasberg M (2003) Characterization of Pt-based catalyst materials by voltammetric techniques. J Power Sources 118:325
12. Cunha EM, Ribeiro J, Kokoh KB, Andrade AR (2011) Preparation, characterization and application of Pt–Ru–Sn/C trimetallic electrocatalysts for ethanol oxidation in direct fuel cell. Int J Hydrogen Energ 36:11034
13. Bagchi J, Bhattacharya SK (2007) The effect of composition of Ni-supported Pt–Ru binary anode catalysts on ethanol oxidation for fuel cells. J Power Sources 163:661
14. Lee C-G, Umeda M, Uchida I (2006) Cyclic voltammetric analysis of C_1–C_4 alcohol electrooxidations with Pt/C and Pt–Ru/C microporous electrodes. J Power Sources 160:78
15. Jiang S, Zhu L, Ma Y, Wang X, Liu J, Zhu J, Fan Y, Zou Z, Hu Z (2010) Direct immobilization of Pt–Ru alloy nanoparticles on nitrogen-doped carbon nanotubes with superior electrocatalytic performance. J Power Sources 195:7578
16. Xi J, Wang J, Yu L, Qiu X, Chen L (2007) Facile approach to enhance the Pt utilization and CO-tolerance of Pt/C catalysts by physically mixing with transition-metal oxide nanoparticles. Chem Commun 16:1656
17. Zhou Y, Gao Y, Liu Y, Liu J (2010) High efficiency Pt–CeO_2/carbon nanotubes hybrid composite as an anode electrocatalyst for direct methanol fuel cells. J Power Sources 195:1605
18. Eguiluz KIB, Malpass GRP, Pupo MMS, Salazar-Banda GR, Avaca LA (2010) Synthesis, characterization and electrocatalytic activity toward methanol oxidation of carbon supported Pt_x–$(RuO_2$–$M)_{1-x}$ composite ternary catalysts (M = CeO_2, MoO_3 or PbO_x). Energy Fuel 24:4012
19. Ou DR, Mori T, Togasaki H, Takahashi M, Ye F, Drennan J (2011) Microstructural and metal-support interactions of the Pt–CeO_2/C catalysts for direct methanol fuel cell application. Langmuir 27:3859
20. Matolín V, Johánek V, Skoda M, Tsud N, Prince KC, Skála T, Matolínová I (2010) Methanol adsorption and decomposition on Pt/CeO_2(111)/Cu(111) thin film model catalyst. Langmuir 26:13333
21. Bai Y, Wu J, Qiu X, Xi J, Wang J, Li J, Zhu W, Chen L (2007) Electrochemical characterization of Pt–CeO_2/C and Pt–$Ce_xZr_{1-x}O_2$/C catalysts for ethanol electro-oxidation. Appl Catal B Environ 73:144
22. De Souza RFB, Flausino AEA, Rascio DC, Oliveira RTS, Teixeira-Neto E, Calegaro ML, Santos MC (2009) Ethanol oxidation reaction on $PtCeO_2$/C electrocatalysts prepared by the polymeric precursor method. Appl Catal B Environ 91:516
23. Calegaro ML, Suffredini HB, Machado SAS, Avaca LA (2006) Preparation, characterization and utilization of new electrocatalyst for ethanol oxidation obtained by the sol–gel method. J Power Sources 156:300
24. Salazar-Banda GR, Suffredini HB, Calegaro ML, Tanimoto ST, Avaca LA (2006) Sol–gel-modified boron-doped diamond surfaces for methanol and ethanol electro-oxidation in acid medium. J Power Sources 162:9
25. Salazar-Banda GR, Suffredini HB, Avaca LA (2005) Improved stability of PtO_x sol–gel-modified diamond electrodes covered with a Nafion® film. J Brazil Chem Soc 16:903
26. Suffredini HB, Salazar-Banda GR, Tanimoto ST, Calegaro ML, Machado SAS, Avaca LA (2006) AFM studies and electrochemical characterization of boron-doped diamond surfaces modified with metal oxides by the sol–gel method. J Braz Chem Soc 17:257
27. Dean AJ (1985) Lange's handbook of chemistry, 13th edn. McGraw-Hill, New York
28. Long JW, Stroud RM, Swider-Lyons KE, Rolison DR (2000) How to make electrocatalysts more active for direct methanol oxidation-avoid PtRu bimetallic alloys. J Phys Chem B 104:9772
29. Cao L, Scheiba F, Roth C, Schweiger F, Cremers C, Stimming U, Fuess H, Chen LQ, Zhu WT, Qiu XP (2006) Novel nanocomposite Pt/$RuO_{2-x}H_2O$/carbon nanotube catalysts for direct methanol fuel cells. Angew Chem Int 45:5315
30. Huang SY, Chang C-M, Wang K-W, Yeh C-T (2007) Promotion of platinum–ruthenium catalyst for electrooxidation of methanol by crystalline ruthenium dioxide. ChemPhysChem 8:1774
31. Eguiluz KIB, Salazar-Banda GR, Miwa D, Machado SAS, Avaca LA (2008) Effect of the catalyst composition in the $Pt_x(Ru$–$Ir)_{1-x}$/C system on the electro-oxidation of methanol in acid media. J Power Sources 179:42
32. Ma J-H, Feng Y–Y, Yu J, Zhao D, Wang A-J, Xu B-Q (2010) Promotion by hydrous ruthenium oxide of platinum for methanol electro-oxidation. J Catal 275:34
33. De Souza RFB, Parreira LS, Silva JCM, Simões FC, Calegaro ML, Giz MJ, Camara GA, Neto AO, Santos MC (2011) PtSnCe/C electrocatalysts for ethanol oxidation: DEFC and FTIR "in situ" studies. Int J Hydrogen Energ 36:11519
34. Christie JH, Lauer G, Osteryoung RA, Anson FC (1963) Determination of charge passed following application of potential step in study of electrode processes. Anal Chem 35:1979
35. Jiang J, Kucernak A (2003) Electrooxidation of small organic molecules on mesoporous precious metal catalysts II: CO and methanol on platinum–ruthenium alloy. J Electroanal Chem 543:187
36. Müller JT, Urban PM, Hölderich WF (1999) Impedance studies on direct methanol fuel cell anodes. J Power Sources 84:157
37. Mancharan R, Goodenough JR (1992) Methanol oxidation in acid on ordered NiTi. J Mater Chem 2:875
38. Salazar-Banda GR, Eguiluz KIB, Pupo MMS, Suffredini HB, Calegaro ML, Avaca LA (2012) The influence of different co-catalysts in Pt-based ternary and quaternary electro-catalysts on the electro-oxidation of methanol and ethanol in acid media. J Electroanal Chem 668:13
39. Murthy A, Manthiram A (2012) Application of derivative voltammetry in the analysis of methanol oxidation reaction. J Phys Chem C 116:3827
40. Murthy A, Lee E, Manthiram A (2012) Electrooxidation of methanol on highly active and stable Pt–Sn–Ce/C catalyst for direct methanol fuel cells. Appl Catal B Environ 121–122:154
41. Hitmi H, Belgsir EM, Léger J-M, Lamy C, Lezna RO (1994) A kinetic analysis of the electro-oxidation of ethanol at a platinum electrode in acid medium. Eletrochim Acta 39:407
42. Roth C, Papworth A, Hussain I, Nichols R, Schiffrin DA (2005) A Pt/Ru nanoparticulate system to study the bifunctional mechanism of electrocatalysis. J Electroanal Chem 581:79

43. Scott FJ, Mukerjee S, Ramaker DE (2007) CO coverage/oxidation correlated with PtRu electrocatalyst particle morphology in 0.3 M methanol by in situ XAS. J Electrochem Soc 154:A396
44. Yuan Q, Zhou Z, Zhuang J, Wang X (2010) Seed displacement, epitaxial synthesis of Rh/Pt bimetallic ultrathin nanowires for highly selective oxidizing ethanol to CO_2. Chem Mater 22:2395
45. Wang H, Jusys Z, Behm RJ (2006) Ethanol electro-oxidation on carbon-supported Pt, PtRu and Pt3Sn catalysts: a quantitative DEMS study. J Power Sources 154:351
46. Camara GA, de Lima RB, Iwasita T (2005) The influence of PtRu atomic composition on the yields of ethanol oxidation: a study by in situ FTIR spectroscopy. J Electroanal Chem 585:128
47. Melke J, Schoekel A, Dixon D, Cremers C, Ramaker DE, Rot C (2010) Ethanol oxidation on carbon-supported Pt, PtRu, and PtSn catalysts studied by operand X-ray absorption spectroscopy. J Phys Chem C 114:5914
48. Tripkovic AV, Popovic KD, Lovic JD (2001) The influence of the oxygen-containing species on the electrooxidation of the C1–C4 alcohols at some platinum single crystal surfaces in alkaline solution. Electrochim Acta 46:3163
49. Xu C, Shen PK, Ji X, Zeng R, Liu Y (2005) Enhanced activity for ethanol electrooxidation on Pt–MgO/C catalysts. Electrochem Comm 7:1305
50. Suffredini HB, Salazar-Banda GR, Avaca LA (2009) Carbon supported electrocatalysts prepared by the sol–gel method and their utilization for the oxidation of methanol in acid media. J Sol-Gel Sci Technol 49:131